Uncertainty in projected critical soil moisture values in CMIP6 affects the interpretation of a more moisture-limited world

Hsin Hsu[1] (hhsu@gmu.edu) and Paul A. Dirmeyer[1,2]

[1]George Mason University, Fairfax, VA, USA

[2]Center for Ocean-Land-Atmosphere Studies, George Mason University, Fairfax, VA, USA

Key points:

- An increasingly moisture-limited world under global warming depends on more than just reduced soil moisture
- Earth system models inconsistently simulate the critical soil moisture value that separates moisture-limited and energy-limited regimes
- Poor agreement among models on projected changes in critical soil moisture calls for greater focus on its observation and validation

Abstract

Evaporation is controlled by soil moisture (SM) availability when conditions are not extremely wet. In such a moisture-limited regime, land-atmosphere coupling is active, and a chain of linked processes allow land surface anomalies to affect weather and climate. How frequently any location is in a moisture-limited regime largely determines the intensity of land feedbacks on climate. Conventionally this has been quantified by shifting probability distributions of SM, but the boundary between moisture-limited and energy-limited regimes, called the critical soil moisture (CSM) value, can also change. CSM is an emergent property of the land-atmosphere system, determined by the balance of radiative, thermal and kinetic energy factors. We propose a novel framework to separate the contributions of these separate effects on the likelihood that SM lies in the moisture-limited regime. We confirm that global warming leads to a more moisture-limited world. This is attributed to reduced SM in most regions: the moisture effect. CSM changes mainly due to shifts in the surface energy budget, significantly affecting 27% of the globe in analyzed climate change simulations. However, consistency among Earth system models regarding CSM change is low. The poor agreement hints that variability of CSM in models and the factors that determine CSM are not well represented. The fidelity of CSM in Earth system models has been overlooked as a factor in water cycle projections. Careful assessment of CSM in nature and for model development should be a priority, with potential benefits for multiple research fields including meteorology, hydrology, and ecology.

Plain Language Summary

In the water cycle, moisture-limited conditions exist when evaporation is limited by a lack of soil moisture. This occurs when soil moisture lies below a threshold called the critical soil moisture (CSM). As evaporation affects atmospheric temperature and humidity, the value of CSM is important for weather and climate, as it determines when land states can affect the atmosphere. Climate change simulations agree the world will become more moisture-limited, mainly attributed to drying soils, but the value of CSM can also change because it is determined in part by local meteorology as part of a land-atmosphere feedback. This study shows that simulations from different climate change models consistently agree on an overall drying of the soil in the future. Changes in CSM are also simulated, but Earth system models do not agree on the magnitude or direction of CSM change in most places. This disagreement introduces uncertainty in the places and times when soil moisture controls evaporation and its impact on the atmosphere. Models have not historically been calibrated or validated for CSM simulation; we advocate for more attention to be paid to observing and modeling CSM due to its importance for meteorology, hydrology, and ecology in a changing climate.

1. Introduction

Coupling between soil moisture (SM) and evaporation, quantified by surface latent heat fluxes (LE), controls the exchange of water and energy across the interface between land and atmosphere (Entekhabi et al. 1996; Bonan 2008b; Santanello et al. 2018). Therefore, SM:LE coupling is one of the most important components of the Earth system (Seneviratne et al. 2010). Observational and model studies have shown that SM extremes can affect weather and climate through this coupling. For example, LE can decrease during drying SM conditions, with a concomitant increase in sensible heat flux, resulting in a warming of air temperature (Schär et al. 1999; Miralles et al. 2014; Koster et al. 2004; Santanello et al. 2005; Dirmeyer 2011; Dirmeyer et al. 2012). Variations in moisture and heat input from land to the atmosphere alters the likelihood and location of precipitation (Ookouchi et al. 1984; Eltahir and Bras, 1996; Findell and Eltahir 1997; Eltahir 1998; Koster et al. 2003; Taylor and Ellis 2006; Taylor et al. 2011; Taylor et al. 2012; Froidevaux et al. 2014; Guillod et al. 2015; Yin et al. 2015; Hsu et al. 2016; Sehler et al. 2020). These SM-driven effects on temperature and precipitation play important roles in extreme events such as heatwaves, droughts and floods (Zaitchik et al. 2006; Fischer et al. 2007; Hirschi et al. 2011; Herold et al. 2016; Miralles et al. 2014; Miralles et al. 2019; Lo et al. 2021; Benson and Dirmeyer 2021; Dirmeyer et al. 2021; Schumacher et al. 2022). Regions that usually experience strong variability in SM and strong control of LE by SM are identified as “hot spots” of land-atmosphere interactions (Koster et al. 2004; Koster et al. 2006; Zhang et al. 2008; Dirmeyer 2011; Diro et al. 2014; Hirschi et al. 2014; Liu et al. 2014; Lorenz et al. 2015; Hsu and Dirmeyer 2021&2022).

However, SM:LE coupling is not active all the time (Budyko 1974; Koster and Milly 1997; Eagleson 1978; Santanello et al. 2007; Zeppetello et al. 2019). Active coupling requires SM content to be below the value of critical soil moisture (CSM), which is the threshold separating regimes where LE is limited by the availability of energy versus water. When SM>CSM, LE variability is governed by the available energy to drive evaporation (Dirmeyer et al. 2000; Feldman et al. 2022). This is called the energy-limited regime. When SM<CSM, LE declines as SM decreases, thus SM:LE coupling becomes active. This is called the moisture-limited regime. Consequently, any location can be classified as more energy-limited or more moisture-limited by examining the number of days spent in each regime. For example, semi-arid regions such as the Sahel have sufficient available incoming radiation but typically moderate to low soil wetness conditions, so are usually in the moisture-limited regime (Koster et al. 2004; Dirmeyer 2011). Combined with strong variance in SM and LE, these regions emerge as some of the strongest hot spots for land-atmosphere interactions. Accordingly, the covariance between SM and LE is a measure of the strength of land-atmosphere coupling (Koster et al. 2004; Dirmeyer 2011).

As soil wetness variations can modify the moisture content and temperature of the near surface atmosphere, thereby impacting extreme events, studies have been devoted to investigating future projections of SM and land-atmosphere coupling under a warming climate (Huszár et al. 1999; Joo et al. 2020; Zhou et al.

2021). By following the customarily-used metrics based on covariances of SM and LE regardless of regime, indices representing the climatological strength of land-atmosphere coupling in a projected climate have been compared to that of current and pre-industrial climate. Most of these studies have suggested a more strongly land-atmospheric coupled world (Ukkola et al, 2018; Dirmeyer et al 2012, 2013, 2022; Seneviratne et al. 2006). However, examining the climatological response of coupling strength without quantifying the day-to-day changes in coupling provides only a partial picture. This is because there are two potential causes for an increase in climatological coupling strength: (1) stronger sensitivity of LE to variations in SM within the moisture-limited regime; (2) a larger proportion of days spent in the moisture-limited regime. That is, stronger SM:LE coupling does not necessarily indicate that variations in SM more strongly determine fluctuations in LE. Rather, it could be that SM drops more frequently below CSM, so that there are more days when SM:LE are coupled, resulting in a larger climatological coupling strength. Of course, both factors could be changing, possibly in opposite directions with regard to their effect on climatological land-atmosphere coupling. To clarify this, attention must also be paid to identifying how the dominant coupling regime can change under global warming. Such an examination reveals different aspects of land-atmosphere coupling.

Diagnosing shifts among SM regimes can be more informative than only calculating the change in SM climatology or distribution. For example, although most climate models project the Amazon basin to become drier under global warming, this does not ensure that the Amazon basin will become more moisture-limited as CSM may also shift. In other words, changes in the dominant SM regime cannot confidently be reflected solely by changes in the local SM distribution. Intuitively, a drying land surface should lead to more moisture-limited conditions; however, this presumes CSM is stationary. The tendency toward more moisture-limited or energy-limited days can also be attributed to a change in the value of CSM. For example, even though the SM distribution of a location remains identical after warming, a higher value of CSM increases the range of SM values identified as moisture-limited, making the location trend toward being climatologically more moisture-limited. Under global warming, such changes in CSM can be anticipated. This is because CSM is not only determined by soil properties and vegetation cover but also meteorological elements of surface energy such as net surface radiation, wind speed (kinetic energy that determines turbulent transfer), and near surface air temperature as well as humidity and its modulation of evaporation (Haghighi et al. 2018).

Thus, it is an open question whether a change in SM distribution or shifting CSM predominantly causes change in the land-atmosphere coupling regime at a given location. To solve this conundrum, it is necessary to diagnose what portion of the shifted SM distribution drops below a shifted CSM. This requires an accurate quantification of CSM. Based on the conceptual frameworks of Budyko (1974) and Seneviratne et al. (2010), different approaches have been proposed. The widely used soil moisture drydown framework (Koster et al. 2009; Gianotti et al. 2019; Feldman et al. 2019) identifies the CSM by finding the value of soil wetness below which the rates of soil wetness decline become significantly

slower, as less evapotranspiration occurs with decreasing SM when WP<SM<CSM. Meanwhile, Schwingshackl et al. (2017) estimated CSM statistically in observational data by seeking the value of soil wetness that optimally separates the relationship between SM and surface heat flux between a positive linear relationship to its dry side and no relationship to its wet side. Denissen et al. (2020) determined CSM by finding the crossover value of soil wetness at which anomalies in evapotranspiration (ET; mass flux converted from LE) are equally correlated to energy and water availability assuming ET depends more on water availability than energy availability when SM<CSM, and vice versa when SM>CSM. Such determinations of CSM and the resulting inferences regarding land-atmosphere coupling in different SM regimes have opened new horizons for the study and understanding of these coupled processes.

Using such approaches, SM regimes have been diagnosed for the current era and examine under projected climate change (Hsu and Dirmeyer 2023; Densissen et al. 2022). Quantification of CSM and its variations is rarely discussed in the Earth science context, even though it is as informative impactful on the water cycle over land as SM or precipitation. In this study, we propose a novel framework that only uses SM and LE data to derive CSM and determine how it contributes to shifts in preferred land-atmosphere coupling regime under global warming. This is achieved by separating how much the change in the frequency of occurrence of moisture-limited days (daily SM below CSM) is due to changes in SM distributions versus the value of CSM. In this context, the change in preferred coupling regime indirectly infers shifts in the activeness of land-atmosphere coupling. The contribution from the changes in SM distribution is referred to as the "moisture effect" since SM content stems directly from the balance of the water budget at the land surface. The contribution from shifts in CSM is termed the "energy effect" since CSM is determined to a large degree by radiative, thermal and kinetic energy budget terms that affect the efficiency of evaporation, which are projected to have a large response to increasing CO_2 in many regions.

2. Data

Daily soil moisture (SM) and latent heat flux (LE) output data are taken from the 1pctCO2 simulation (Eyring et al. 2016) of 15 climate models participating CMIP6 (AWI-ESM-1-1-LR, CanESM5, CMCC-ESM2, CNRM-CM6-1, CNRM-CM6-1-HR, INM-CM4-8, MIROC-ES2L, MRI-ESM2-0, CMCC-CM2-SR5, MPI-ESM-1-2-HAM, ICON-ESM-LR, IPSL-CM6A-LR, GFDL-CM4, NorESM2-MM, MIROC6) as displayed in Table 1. We use ensemble member r1i1p1f1 from all models, except for CNRM-CM6-1-HR, from which member r1i1p1f2 is used. These simulations cover at least 150 years with gradually increasing concentrations of CO_2 at a rate of 1% per year. Analysis is performed for the first 20 years (1^{st} to 20^{th}; hereafter called the pre-warming period) and the last 20 years (130^{th} to 150^{th}; hereafter called the post-warming period) to examine the response of the preferred regime under warming and the moisture and energy effects contributing to it. To minimize the effect of frozen or snow covered days that might adversely affect the determination of SM:LE relationships, daily data from May to September (MJJAS) for regions between 23°N-60°N, November to

March (NDJFM) for regions between 23°S-60°S, and all months for regions between 23°S-23°N are used. Regions poleward of 60° are not included in this analysis.

3. Methods

3.1 Critical soil moisture determination

For each grid cell in the output of a climate model, we estimate CSM for each analyzed time period by piecewise linear regression. By theorem, a full SM:LE relationship can be separated into three ranges by two critical values. Each regime bears different SM:LE behavior. CSM separates SM into an energy-limited regime (also known as the wet regime) and a moisture-limited regime. Another critical value, the wilting point (WP), separates the moisture-limited regime into dry and transitional regimes. Consequently, the full SM range consisting of an energy-limited regime and a moisture-limited regime can also be described as a three-phase set of regimes: dry, transitional and wet. Within this conceptualization, WP and CSM are determined by selecting the best fitting among five possible piecewise linear regressions, as displayed in Figure 1:

Regression A: A zero slope followed by a positive slope followed by a zero slope: Both WP and CSM are evident within the SM distribution, which is separated into a zero SM:LE correlation on the dry side of WP and the wet side of CSM. Between WP and SM, the SM:LE correlation is positive. For this case, the SM distribution lies partially within the moisture-limited regime and the value of CSM can be determined.

Regression B: A positive slope followed by a zero slope: Only the CSM is evident within the SM distribution, which is separated into a positive SM:LE correlation on the dry side of CSM and a zero SM:LE correlation on the wet side of CSM. For this case, the SM distribution lies partially within the moisture-limited regime, and the value of CSM is again identifiable.

Regression C: A zero slope followed by a positive slope: Only the WP is evident within the SM distribution, which is separated into a zero SM:LE correlation on the dry side of WP and a positive SM:LE correlation on the wet side of WP. The SM distribution lies completely within the moisture-limited regime and the value of the CSM cannot be determined.

Regression D: A zero slope throughout: neither WP nor CSM are identifiable within the SM distribution, and only one regime exists. Such locations are found mostly over moist tropical rainforests, high-latitude and alpine areas, we assume the SM distribution lies totally within the energy-limited regime and CSM lies at the drier side of the SM distribution. The value of CSM is not identifiable by this regression.

Regression E: A positive slope throughout: neither WP nor CSM are identifiable within the SM distribution. As LE is positively correlated to SM,

the SM distribution lies totally within the transitional regime and thus the moisture-limited regime. The value of CSM lies at the wetter side of SM but its value cannot be determined.

For each grid cell and each CMIP6 model, we fit each of the above piecewise regressions to the SM:LE daily data. The best fitting regression is selected by BIC (Bayesian information criterion; Schwarz 1978). As we aim to examine how a location becomes more moisture-limited or energy-limited, changes in CSM and its separating SM regimes are our focus. Although WP is relevant to phytology and global warming can impact vegetation, land-cover changes are not included in 1pctCO2 simulations, so we do not examine changes in WP. Moreover, not all climate models incorporate full dynamic vegetation models, which describe how natural vegetation coverage and competition responses to climate change. These non-representative land conditions preclude discussion of changes in WP under warming. Furthermore, the value of WP does not affect how many days in a period can be identified as moisture-limited.

3.2 Quantifying moisture and energy effects

Figure 2 is a schematic plot showing the calculation of percentage of days identified as moisture-limited (P_{ML}) and energy-limited (P_{EL}), and contributions of the moisture effect (P_{ME}) and the energy effect (P_{EE}). $P_{[a,b]}$ indicates the probability of soil moisture falling within the range between a and b. Variables with a prime are quantities for the post-warming period; $a = min$ or $b = MAX$ indicate the minimum and maximum value of SM during the analyzed period, respectively.

If a valid value of CSM is detected in an analyzed period, we calculate $P_{ML} = P_{[min,CSM]}$ (yellow shading in Fig1a) and $P_{EL} = P_{[CSM,MAX]}$ (orange shading in Fig1a). Under warming, the probability distribution of SM may be different, as may be P_{ML} and P_{EL}. The change in the percentage of days identified as moisture-limited (ΔP_{ML}) can be written as $\Delta P_{ML} = P'_{ML} - P_{ML}$. This can further be decomposed into the contributions from moisture effect and energy effect; thus: $\Delta P_{ML} = P_{EE} + P_{ME}$.

Assuming CSM does not change under warming (Fig2), ΔP_{ML} is due solely to the moisture effect $P_{ME} = P'_{[min,CSM]} - P_{[min,CSM]}$ (peach shading minus aqua shading in Fig1b). The remaining change in P_{ML}, after accounting for the moisture effect P_{ME}, is contributed by the energy effect $P_{EE} = P'_{[CSM,CSM']}$ (purple shading in Fig3). Note that the analysis here only holds for the grid cell where CSM is detected in both periods. For locations where CSM emerges or vanishes between the periods, we are unable to separate the contributions of the moisture effect and energy effect. As a result, across all climate models, only ~30% of the grid cells over land contribute to this analysis.

If a value of CSM is detected both in the pre- and post-warming periods, a chi-square test to determine the significance of ΔCSM is applied. The null hypothesis is that the fraction of SM during the pre-warming period that lies below the pre-warming value of CSM ($P_{[min,CSM]}$) is equal to that below the

post-warming CSM' ($P_{[min,CSM']}$). Note that only the SM distribution from the pre-warming period is used here.

To test the significance of $\Delta P_{ML} = P'_{ML} - P_{ML}$, if CSM is detected both in the pre- and post-warming periods, the chi-square test with a subtly different null hypothesis is applied. Here, we test the equivalence of the fractions of daily SM values below the corresponding CSM between the two periods ($P_{[min,CSM]}$ and $P'_{[min',CSM']}$). That is, we test if the fraction of SM during the pre-warming period that lies below the pre-warming CSM value ($P_{[min,CSM]}$) is significantly different from the fraction of SM during the post-warming period that lies below the post-warming CSM' ($P'_{[min',CSM']}$). Note that P_{ML} is equivalent to the percentile value of CSM within the given SM probability distribution. This enables the rationale of applying a similar statistical significance test between ΔCSM and ΔP_{ML}.

4. Results and Discussion

The global patterns of the change in SM climatology (kg/m^2) between pre- and post-warming periods in each climate model are displayed in Figure 3. Only the grid cells where $p<0.05$ by a Student's t-test are shaded. The column *a* of Table 2 displays the summation of drying areas (brown shaded areas in Figure 3) and wetting areas (green shading areas in Figure 3) for each climate model. A tendency of SM toward drier conditions is revealed globally in most models. Drying responses are often seen over the Amazon, the conterminous U.S, areas of Europe, China, the Sahara, and southern Africa. Wetting responses are seen over many high latitude areas, the Pampas, eastern Africa, and India.

Figure 4 shows the global patterns of the change in CSM (kg/m^2). Only grid cells with $p<0.05$ determined by a chi-squared test are shaded. In addition, we label the locations where CSM disappears from present to future climate by green dots. Locations with an emerging CSM are labeled by purple dots. Unlike the results for SM, changes in CSM do not have a strong multi-model global tendency under global warming (Column *b* of Table 2). Nevertheless, they do show structured patterns; regionally consistent patterns in terms of the sign of the CSM change can be seen in individual climate models. For example, most climate models project a consistent change in CSM over Australia, where higher values of CSM are seen in CNRM-CM6-1, AWI-ESM-1-1-LR, NorESM2-MM, MPI-ESM-1-2-HAM, and INM-CM4-8 but opposite responses are evident in MIROC-ES2L, GFDL-CM4, and CanESM5. A similar situation can be found over the Amazon, the Sahel and India. These indicate a lack of consensus among climate models of how hydroclimate interacts with global warming. CSM emerges (green dots) over the Amazon from areas that were consistently in the wet regime in several climate models. This is likely because the overall drying SM tendency leads soil wetness conditions to decline in the moisture-limited regime. CSM is also emerging in many parts of the mid- and high-latitudes of the Northern Hemisphere, regardless of whether SM is increasing or declining, as compared to Figure 3. A regional analysis of trends in each climate model's relevant meteorological variables is needed to clarify the specific causes of the projected changes, as they can arise from various aspects of the water and energy cycles.

Additionally, most climate models project only sporadic locations where CSM is vanishing. This indicates that under global warming, the SM distribution tends toward spanning both the moisture- and energy-limited regimes.

The change in moisture-limited days ΔP_{ML} is displayed in Figure 5. Most climate models project a more moisture-limited world (column *c* of Table 2). This implies that land-atmosphere interactions at the day-to-day timescale might become more active because there would be more days when SM:LE coupling is active. Consistent responses are seen over many locations among models. Over the southern Great Plains, which has been identified as a hot spot of land atmosphere coupling (e.g., Koster et al. 2004; Dirmeyer 2011), ~10% more days lie within the range of soil moisture that defines moisture-limited conditions. A similar change is seen over South Africa. Over the Amazon, most climate models project a more moisture-limited (i.e., less energy-limited) climate but several climate models such as CNRM-CM6-1, CNRM-CM6-1-HR, MRI-ESM2-0, and MOROC6 show no change. For these climate models, despite a significant drying response in SM, SM does not drop below the CSM and thus it sticks at energy-limited conditions.

Less moisture-limited climates are mostly found over the monsoon areas of Central Africa and South and Southeast Asia. However, the boundary of these areas varies a lot among climate models. For example, the western part of the Sahel becomes more moisture-limited in some models whereas more energy-limited conditions over the Sahel are seen overall in CMCC-CM2-SR5, CMCC-ESM2 GFDL-CM4, CanESM5, and MPI-ESM-1-2-HAM. This can be attributed to the low consensus in both SM response and CSM response under a warming climate. The same argument can be made for the mid- to high-latitude areas where the response ΔP_{ML} at any location is rarely consistent among climate models. Large ΔP_{ML} is usually found over mid- to high-latitudes; for an extreme case, some climate models show that ΔP_{ML} can be close to 100%. CSM over these areas is usually not identifiable (i.e., it is outside the range of the local SM distribution; Figure 4). Since the response of SM in those areas is also large (Figure 3), it is difficult to determine whether shifts in SM or CSM mainly contribute to such results. Nevertheless, these results indicate that the hydroclimate over mid- to high-latitudes is highly sensitive to global warming.

Figure 6 displays the contribution of the moisture effect P_{ME} (%) and energy effect P_{EE} (%) to ΔP_{ML}. For clarification, a positive P_{ME} contributes to a positive ΔP_{ML} via a drying response in the SM distribution (as in Figure 3). A positive P_{EE} that contributes to a positive ΔP_{ML} corresponds to an increase in the value of CSM in Figure 4. Shading with a two dimensional color scheme is used to indicate which effect locally plays a dominant role. We arbitrarily define that if the magnitude of the contribution of ΔP_{ML} by one effect is 50% larger than the contribution by the other, that larger effect is declared to be dominant. This yields three categories for each location: P_{ME} dominance, P_{EE} dominance, and roughly equal dominance. The percentage of area classified within each category is indicated for each model in column *d* of Table 2.

Over the globe, ΔP_{ML} is dominated by either one of these effects, as the area with equal dominance is the lowest among the three categories for all climate models. All climate models suggest that P_{ME} plays a more important role in more locations, except for NorESM2-MM in which the total area of P_{EE} dominance is slightly larger than for P_{ME}. These moisture effect dominance areas having a positive contribution (red-peach scheme) are found in most models over the Amazon, South Africa, the southern Great Plains, and Mediterranean coastal areas in most models. This corresponds to areas with a drying SM, consistently found among climate models (Figure 3). Note that although P_{ME} is dominant in these areas, P_{EE} is significant, indicating the energy effect is also strong; this is especially true for areas with red shading. Over the East Africa and India, a relatively small ΔP_{ML} results from a negative moisture effect and a positive energy effect. Large discrepancies in both contributing factors are seen among climate models over Australia and the western part of the Sahel, mirroring to the diverse responses of SM and CSM described previously.

The sign of P_{EE} is more diverse among climate models than that of P_{ME}, indicating a discrepancy among models in the simulated energy response of the hydroclimate under global warming. This means that a significant warming of the globe does not necessarily play the same role in affecting shifts in CSM across the climate models. However, the consistent tendency toward a more moisture-limited world and the dominance of the moisture effect in most regions reinforces the finding of past examinations in which a stronger land-atmosphere coupling is found in a projected warming climate. On the other hand, the credibility of that conclusion is tempered by the diversity in the responses of CSM found among the climate models.

The poor agreement on P_{EE} could hint that variability of CSM in climate models could be poorly represented. In nature, CSM is a quantity emerging from multiple processes and factors in/between the land and atmosphere. For example, soil texture and vegetation affect the amount of available energy obtained from solar radiation (e.g., via albedo effects) and the ability of water to escape from the soil (e.g., via the opening of plant stomata or through the joint effects of porosity, permeability, and rooting depth on water availability). Cloud radiative effects or atmospheric radiative transfer affect available energy. Wind speeds and daily atmospheric temperature and humidity profiles act to alter the efficiency of evaporation. However, in climate models, many of these processes are heavily parameterized. This means CSM in the models is a property determined by interactions of multiple parameterizations in both the atmosphere and land components of the Earth system.

The way CSM emerges in nature also indicates that it is not a stationary quantity, but its magnitude at a location can vary temporarily and be affected by climate variability and natural/anthropogenic forcings. Our results hint that the CSM that emerges from the behavior of various parameterizations in the climate models, often without a consistent physical foundation, leads to an unrealistic interaction between CSM and model climate variability. An incorrectly modeled CSM leads to biased partitioning of the climate into moisture-limited and

energy-limited states, which could be the crux of poor model performance across a variety of timescales. For example, even if land surface processes were perfectly represented in a model, a biased CSM would lead to an incorrect determination of daily SM:LE coupling, resulting in a biased atmospheric profile. At the seasonal scale, this induces a bias in the number of days with active land-atmosphere interactions and thus the assessment of the climatology of meteorological fields as well as their assessment under future climate projections.

5. Conclusions

We have examined whether and how the world becomes more moisture-limited under global warming from the perspective of soil moisture controls on surface fluxes. We propose a novel framework to diagnose the contribution of such changes divided into a moisture effect (shifting probability distributions of soil moisture) and an energy effect (shifts in the value of the critical soil moisture that separates moisture-limited surface flux modulation from energy-limited). Under a scenario with increasing CO_2 by 1% per year, after one and a quarter centuries, almost all analyzed climate models suggest a drying SM response and a more moisture-limited world. However, climate models show a greater spread in the response of CSM to warming, although its change is statistically significant over many regions in the low- and mid-latitudes. Moreover, CSM breakpoints emerge in locations in the tropics and mid-high latitudes where they are not evident in pre-warming conditions. These lead to a statistically significant change in the range of SM values identified as moisture-limited and can result in changes in the most common SM regime.

The framework used here to separate moisture and energy effects only uses land-relevant variables. This provides a new method to diagnose the cause of changes in land-atmosphere interactions with a relatively small amount of data. This is of benefit to investigations of climate extremes, hydrology, and phenology, in which variations in land-atmosphere interactions play a crucial role. Results presented here and from past studies (Jung et al. 2010; Dirmeyer et al. 2013; Zhou et al. 2021; Hsu and Dirmeyer 2023) indicating a more-moisture limited world under global warming is brought into question by the large spread of CSM responses among CMIP6 models. Based on this uncertainty in modeled CSM, future studies should put more effort toward examination and validation of CSM. This is a new direction for improving climate model performance as CSM is an emergent environmental property arising from multiple processes taking place at the land surface, in the atmosphere, and within the interface between them.

We emphasize that exploring the moisture budget of the land surface alone is insufficient to describe the whole picture of hydroclimate and its response (e.g. the commonly used $P - E - R$, precipitation minus evaporation minus runoff) under different forcings. Examining factors such as how CSM arises and varies are equally important. CSM determines the behavior of evaporation on SM and thus is key to bridging the water cycle with thermal states at the Earth's surface. The portion of the range of SM that is moisture-limited depends solely on the

local value of CSM. This inherently determines how frequently the atmosphere is sensitive to land conditions, which is in turn affected by atmospheric phenomenon in a feedback cycle that is vulnerable to human activity. Accordingly, the water and energy cycles, weather and climate, ecosystems and society, are all directly or indirectly interconnected to CSM and its variability. Thus, diagnosis of CSM in a changing climate can add critical information along side other customarily analyzed variables such as precipitation, soil moisture, and temperature. Including the discussion of CSM in the context of Earth science provides a more complete perspective of the evolution of Earth system.

Acknowledgements:

This work was supported by National Aeronautics and Space Administration (NASA) grant 80NSSC20K1803.

Data availability:

CMIP6 model data are available at: https://esgf-node.llnl.gov/search/cmip6/.
Variables of the simulations used here can be accessed by checking the boxes in the website as below: Specific model name(Source ID)/1pctCO2(Experiment ID)/day (Frequency)/mrsos and hfls(Variable)
Source code of analysis and plots are available at:
https://zenodo.org/record/7562124#.Y865AXZOlD8

CMIP Label	RES (lat x lon)	Full Citation
AWI-ESM-1-1-LR	1.875x1.875	Semmler, T., & Co-authors (2018). AWI AWI-CM1.1MR model output prepared for CMIP6 CMIP. Earth System Grid Federation. DOI: 10.22033/ESGF/CMIP6.359.
CNRM-CM6-1	1.4x1.4	Voldoire, Aurore (2019). CNRM-CERFACS CNRM-CM6-1-HR model output prepared for CMIP6 HighResMIP. Earth System Grid Federation. DOI: 10.22033/ESGF/CMIP6.1387
CNRM-CM6-1-HR	0.25x0.25	Voldoire, A. (2018). CNRM-CERFACS CNRM-CM6-1 model output prepared for CMIP6 CMIP. Earth System Grid Federation. doi: DOI: 10.22033/ESGF/CMIP6.1375.
INM-CM4-8	1.5x2	Volodin, Evgeny; and co-authors (2019). INM INM-CM4-8 model output prepared for CMIP6 CMIP piControl. Earth System Grid Federation. DOI: 10.22033/ESGF/CMIP6.5080
IPSL-CM6A-LR	1.25x2.5	Boucher, O.; Denvil, S.; Caubel, A.; Foujols, M. A. (2020). IPSL IPSL-CM6A-LR-INCA model output prepared for CMIP6 AerChemMIP. Earth System Grid Federation. DOI: 10.22033/ESGF/CMIP6.13581.
MIROC6	1.4x1.4	Takemura, T. (2019). MIROC MIROC6 model output prepared for CMIP6 AerChemMIP. Earth System Grid Federation. doi: DOI: 10.22033/ESGF/CMIP6.9121.
MIROC-ES2L	1.4x1.4	Tachiiri, Kaoru; and co-authors (2019). MIROC MIROC-ES2L model output prepared for CMIP6 ScenarioMIP..Earth System Grid Federation. DOI: 10.22033/ESGF/CMIP6.936
CMCC-CM2-SR5	1.06x0.8	Lovato, Tomas; Peano, Daniele (2020). CMCC CMCC-CM2-SR5 model output prepared for CMIP6 ScenarioMIP. Earth System Grid Federation. DOI: 10.22033/ESGF/CMIP6.1365
CMCC-ESM2	0.9375x1.25	Lovato, T., & Butenschön, M. (2021). CMCC CMCC-ESM2 model output prepared for CMIP6 OMIP (Version 20210127). Earth System Grid Federation. DOI: 10.22033/ESGF/CMIP6.13167
CanESM5	2.8125x2.8125	Swart, N. C., & Co-authors (2019). CCCma CanESM5 model output prepared for CMIP6 CMIP. (Version 20190502).Earth System Grid Federation. DOI: 10.22033/ESGF/CMIP6.1303
NorESM2-MM	0.9375x1.25	Bethke, I. & Co-authors (2019). NCC NorCPM1 model output prepared for CMIP6 CMIP. Earth System Grid Federation. DOI: 10.22033/ESGF/CMIP6.10843.
MRI-ESM2-0	1.125x1.125	Yukimoto, S. & Co-authors (2019). MRI MRI-ESM2.0 model output prepared for CMIP6 CMIP. Earth System Grid Federation. DOI: 10.22033/ESGF/CMIP6.621
MPI-ESM-1-2-HAM	1.875x1.875	Neubauer, David; and co-authors (2019). HAMMOZ-Consortium MPI-ESM1.2-HAM model output prepared for CMIP6 AerChemMIP.Earth System Grid Federation. DOI: 10.22033/ESGF/CMIP6.1621
ICON-ESM-LR	not gridded	Nicholls, Zebedee, and co-authors, 2021: Regionally aggregated, stitched and de-drifted CMIP-climate data, processed with netCDF-SCM v2.0.0. Geoscience Data Journal, DOI:10.1002/gdj3.113.
GFDL-CM4	0.25x0.25	Guo, Huan; and co-authors (2018). NOAA-GFDL GFDL-CM4 model output. Earth System Grid Federation. DOI: 10.22033/ESGF/CMIP6.1402

Table 1| CMIP models, resolutions (RES; unit: degree) and data citations.

Climate Model	(a) Figure 3 SM responses		(b) Figure 4 CSM responses		(c) Figure 5 ΔPml		(d) Figure 6 Dominant effect		
	Drier	Wetter	Drier	Wetter	More energy -limited	More moisture -limited	Moisture effect	Equally dominant	Energy effect
GFDL-CM4	**55**	37	**20**	7	24	**32**	**19**	5	10
NorESM2-MM	**53**	41	11	**19**	22	**40**	13	5	**14**
MRI-ESM2-0	**66**	26	**9**	8	17	**32**	**26**	3	6
IPSL-CM6A-LR	45	**48**	9	**21**	26	**36**	**21**	6	11
ICON-ESM-LR	**56**	39	**19**	9	21	**36**	**28**	4	6
MPI-ESM-1-2-HAM	43	**50**	10	**16**	25	**33**	**24**	4	7
CanESM5	**66**	29	**17**	14	25	**35**	**28**	4	8
MIROC6	**58**	34	**22**	9	26	**32**	**21**	4	11
MIROC-ES2L	**59**	35	**22**	7	**29**	26	**18**	4	12
INM-CM4-8	41	**48**	5	**16**	21	**33**	**24**	3	9
CNRM-CM6-HR	**56**	37	7	**22**	19	**34**	**20**	5	11
CNRM-CM6-1	**56**	37	7	**18**	18	**31**	**20**	5	8
AWI-SM-1-1-LR	**46**	44	9	**21**	20	**39**	**25**	6	10
CMCC-CM2-SR5	**54**	40	13	**14**	29	**35**	**29**	4	8
CMCC-ESM2	**57**	37	11	**13**	29	**33**	**27**	4	8
Mean	**54.1**	38.8	12.7	**14.3**	23.4	**33.8**	**22.9**	4.4	9.3
Spread	7.5	6.8	5.8	5.3	4	3.4	4.5	0.9	2.3

Table 2| the percentage of land area (60°S to 60°N) (a) with a significantly drying response or wetting response from pre- to post-warming periods, (b) with a significantly drier or a wetter value of CSM in the post-warming period, (c) with significantly decreasing or increasing P_{ML}, and (d) where P_{ML}' is dominated by P_{ME} or by P_{EE} or no dominance. Bold text indicates the spatially dominant (largest percentage) response of a climate model for each specific analysis.

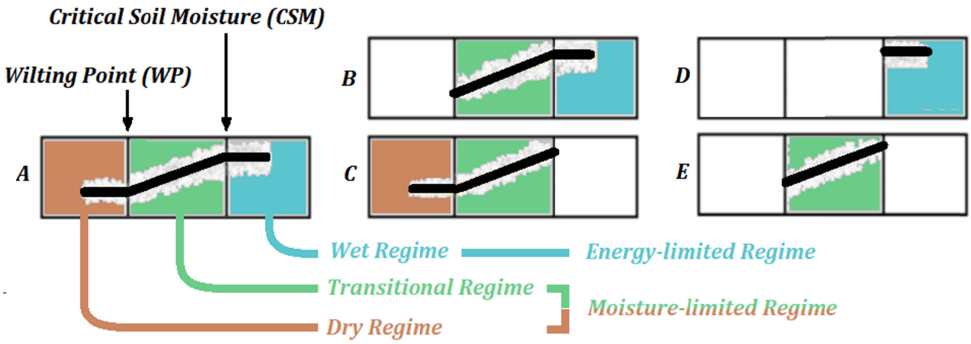

542

544 Figure 1| Five piecewise linear regressions used to represent soil moisture
545 regimes and critical soil moisture values present over any given location.

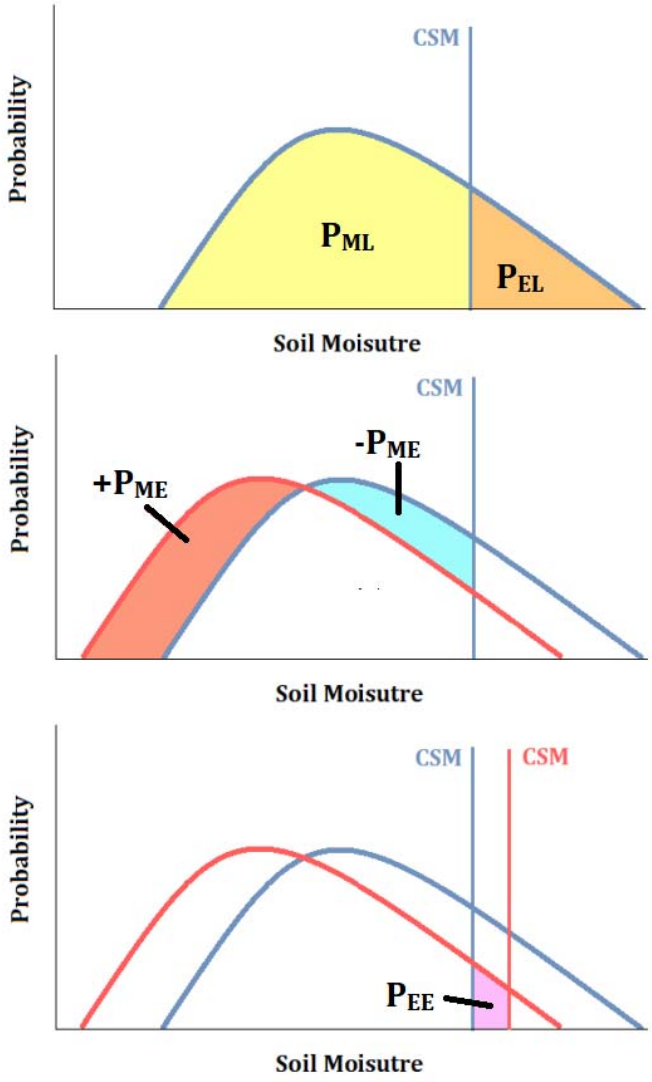

Figure 2| Schematic of the method to quantify the percentage of days in moisture-limited conditions (P_{ML}), and energy-limited conditions (P_{EL}). For a specific location, (a) If CSM is identified in an analyzed period, days with SM drier than CSM are specified as being under moisture-limited conditions (yellow shading) and days with SM wetter than CSM are identified as under energy-limited conditions (orange shading). (b) If the CSM can be determined in both the pre- and post-warming period, change in P_{ML} contributed by the moisture effect (P_{ME}) is quantified as the change in the percentage of days spent in moisture-limited conditions given a CSM defined at the pre-warming period value (red minus blue areas). (c) the change due to the energy effect (P_{EE}) is the change in P_{ML} integrated between the CSM values in the pre- and post-warming periods (purple area).

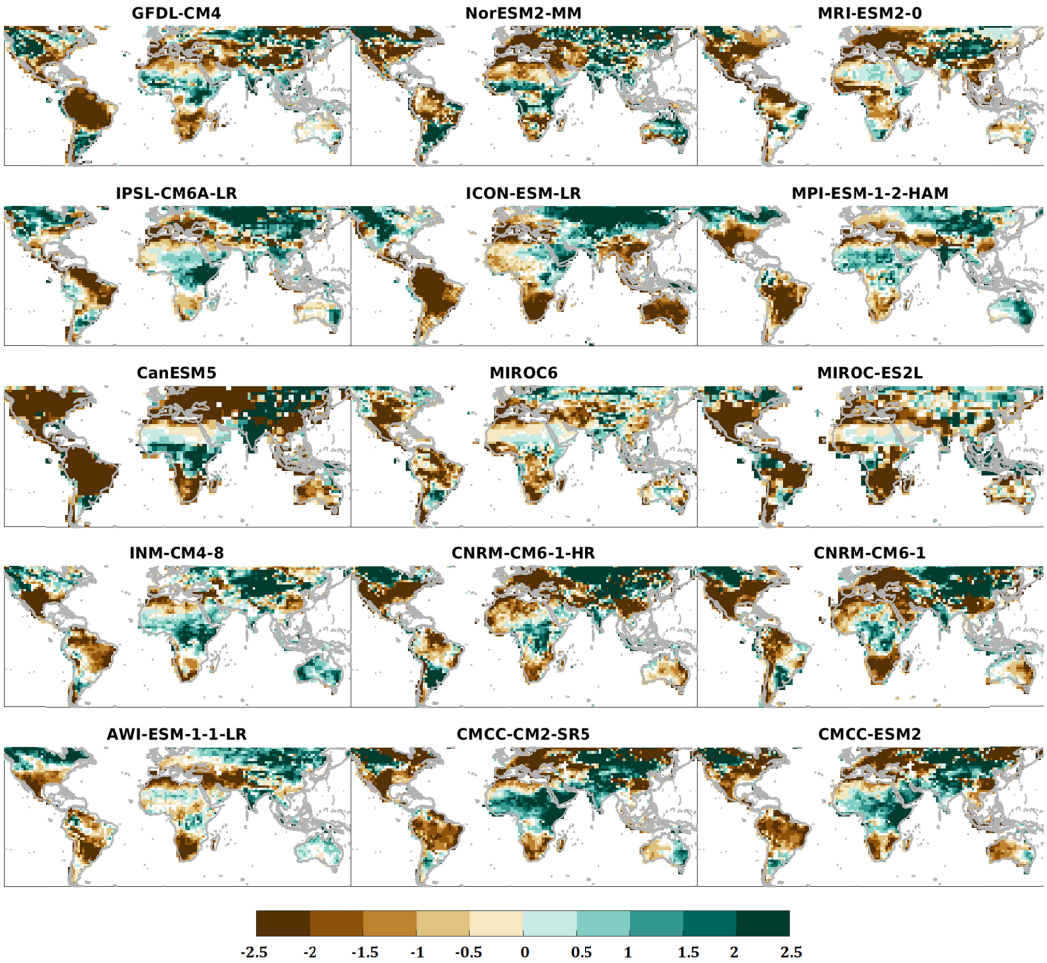

Figure 3| Difference of mean SM (kg/m2) between the two analyzed period (post-warming minus pre-warming, using May to September data for regions between 23°N-60°N, November to March for regions between 23°S-60°S, and all months for regions between 23°S-23°N). Only grid cells that pass a Student's t-test at the 95% confidence level (p-value < 0.05) are shaded.

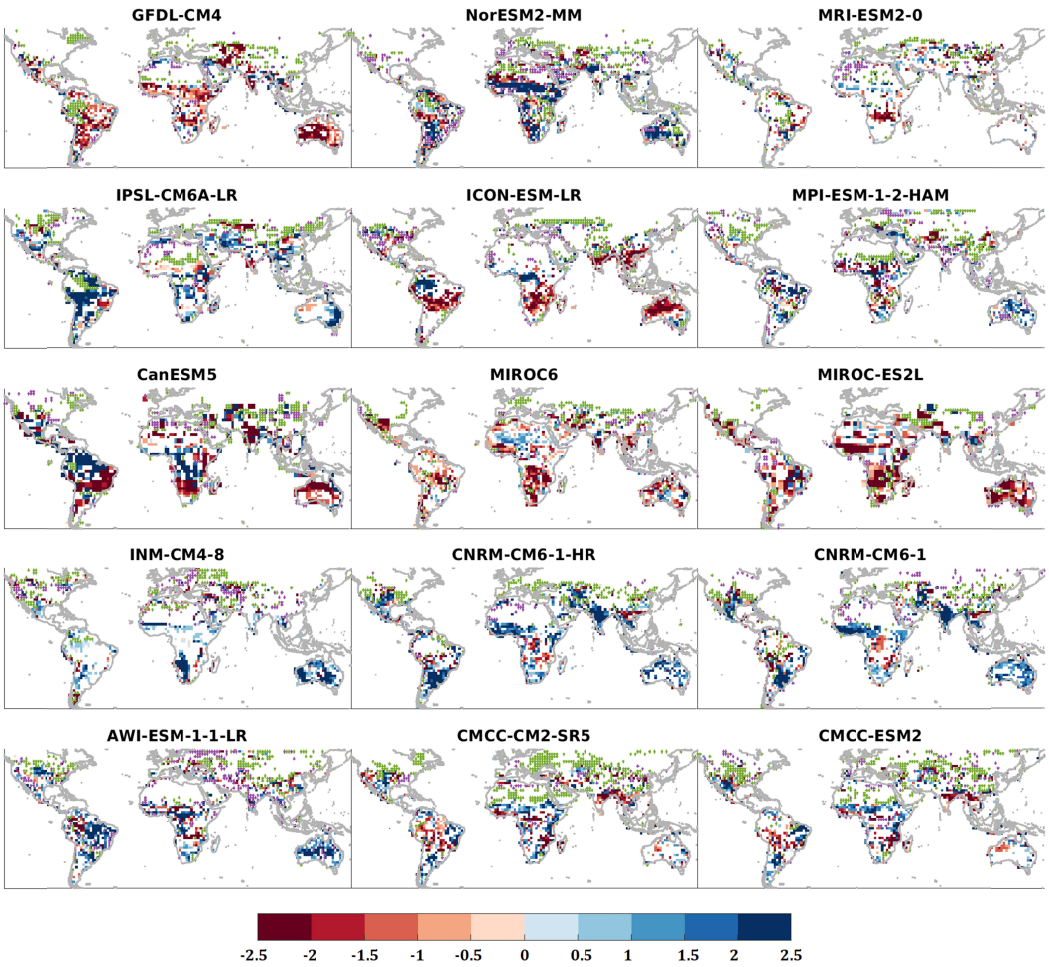

Figure 4| Difference of CSM (kg/m^2) between the two analyzed periods (post-warming minus pre-warming). Only grid cells where a chi-square-test is passed at the 95% confidence level (p-value < 0.05) are shaded; with the hypothesis that the fraction of days when pre-warming SM is drier than the CSM is the same as for post-warming CSM'. Green shading indicates a CSM emerges in post-warming period but is not identifiable from the SM data in the pre-warming period. Purple shading means a CSM value cannot be identified in the post-warming period but is found in the pre-warming period.

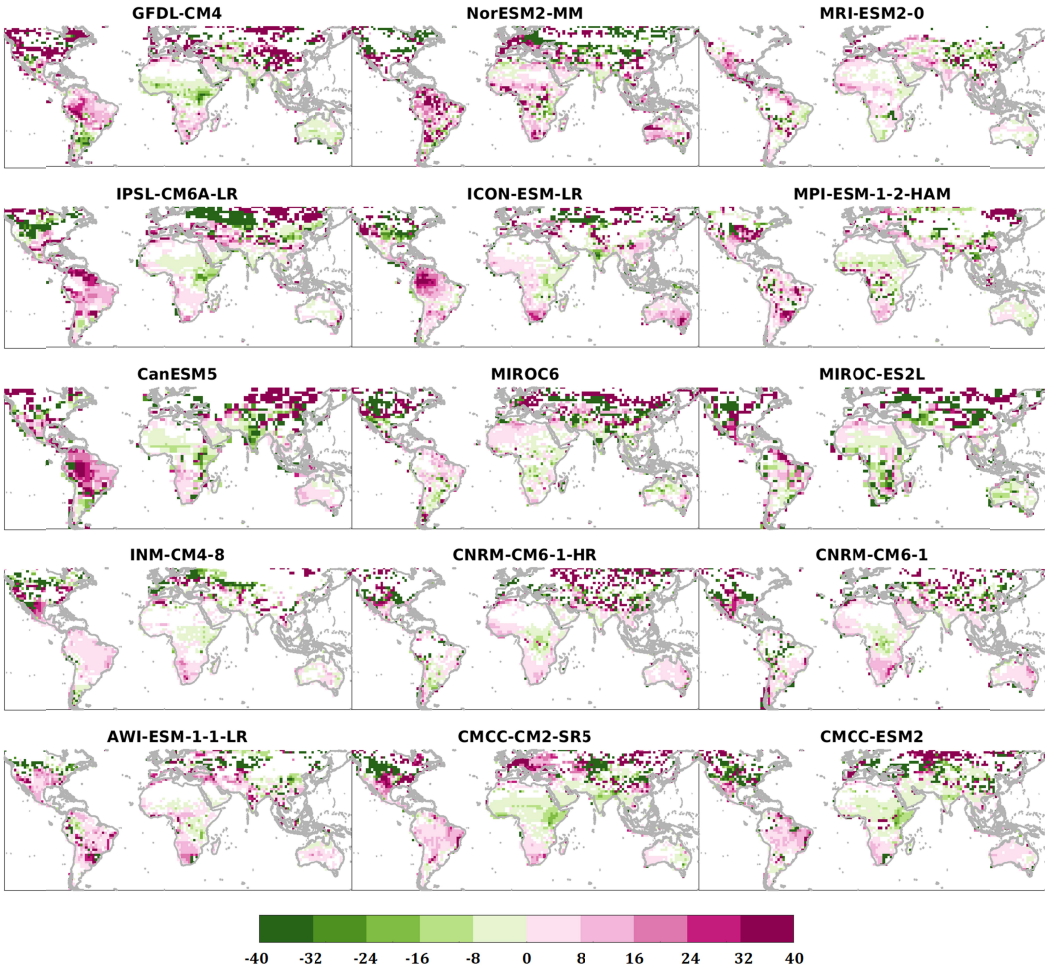

Figure 5| ΔP_{ML} (%) calculated as: P_{ML}' minus P_{ML}. Only grid cells where a chi-square-test is passed at the 95% confidence level (p-value < 0.05) are shaded; with the hypothesis that the fraction of days when SM is drier than CSM is equal between two periods (identical to the test in Figure 6.3).

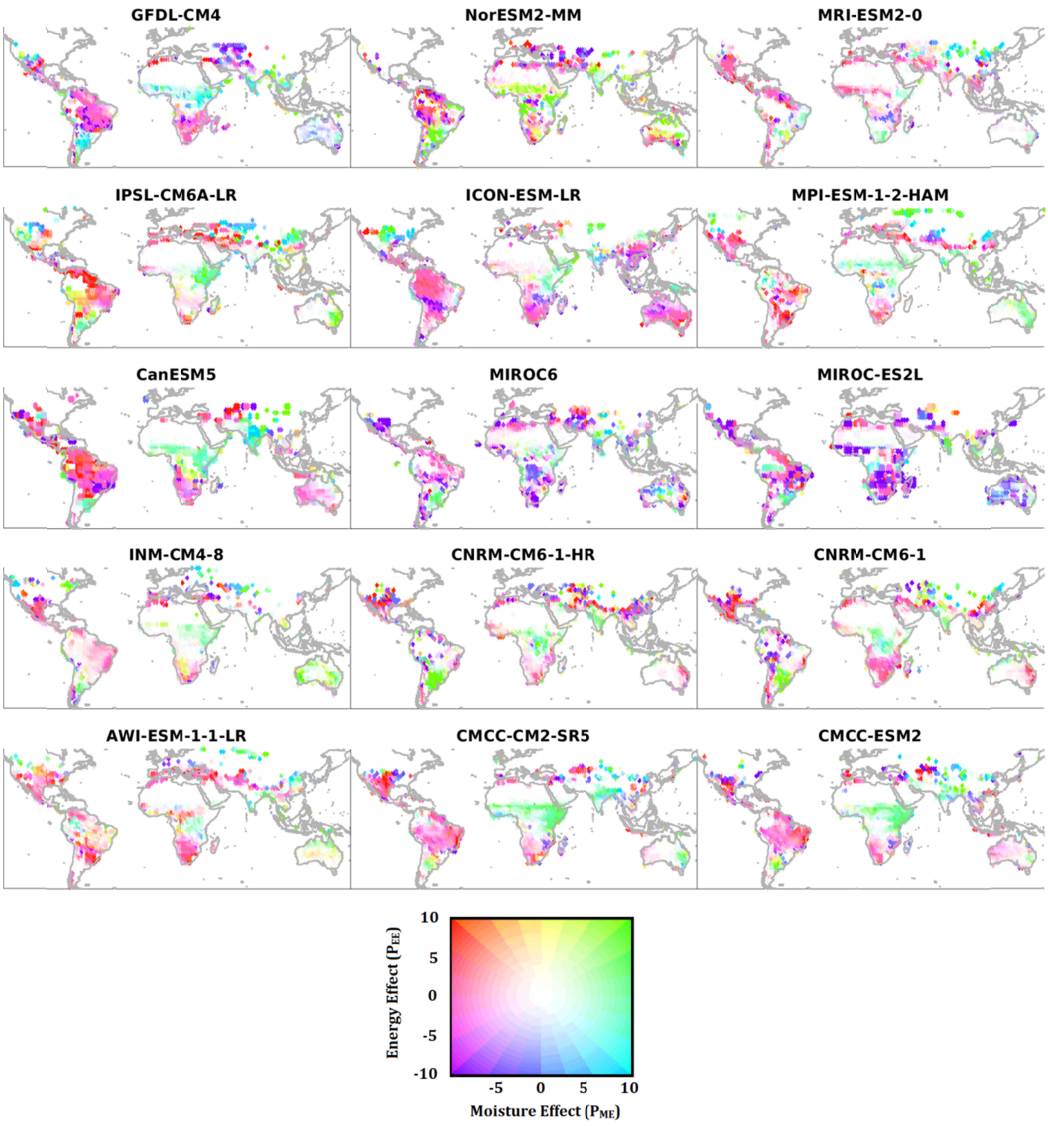

583

587 Figure 6| P_{ME} (%) and P_{EE} (%) contributing to ΔP_{ML}. Grid cells are shaded only if
588 their CSM can be determined in both pre- and post-warming periods and their
589 ΔP_{ML} values are statistically significant. Individual statistical tests are not
590 performed for P_{ME} and P_{EE}, as they are decomposed components of ΔP_{ML}.

588

588

References

1. Benson, D. O. & Dirmeyer, P. A. Characterizing the Relationship between Temperature and Soil Moisture Extremes and Their Role in the Exacerbation of Heat Waves over the Contiguous United States. *Journal of Climate* **34**, 2175–2187 (2021).

2. Berg, A. *et al.* Land–atmosphere feedbacks amplify aridity increase over land under global warming. *Nature Clim Change* **6**, 869–874 (2016).

3. Bonan, G. B. Forests and Climate Change: Forcings, Feedbacks, and the Climate Benefits of Forests. *Science* **320**, 1444–1449 (2008).

4. Byrne, M. P. & O'Gorman, P. A. The Response of Precipitation Minus Evapotranspiration to Climate Warming: Why the "Wet-Get-Wetter, Dry-Get-Drier" Scaling Does Not Hold over Land*. *Journal of Climate* **28**, 8078–8092 (2015).

5. Denissen, J. M. C., Teuling, A. J., Reichstein, M. & Orth, R. Critical Soil Moisture Derived From Satellite Observations Over Europe. *J. Geophys. Res. Atmos.* **125**, (2020).

6. Dirmeyer, P. A. The terrestrial segment of soil moisture-climate coupling: SOIL MOISTURE-CLIMATE COUPLING. *Geophys. Res. Lett.* **38**, n/a-n/a (2011).

7. Dirmeyer, P. A., Balsamo, G., Blyth, E. M., Morrison, R. & Cooper, H. M. Land-Atmosphere Interactions Exacerbated the Drought and Heatwave Over Northern Europe During Summer 2018. *AGU Advances* **2**, (2021).

8. Dirmeyer, P. A. *et al.* Evidence for Enhanced Land–Atmosphere Feedback in a Warming Climate. *Journal of Hydrometeorology* **13**, 981–995 (2012).

9. Dirmeyer, P. A., Jin, Y., Singh, B. & Yan, X. Trends in Land–Atmosphere Interactions from CMIP5 Simulations. *Journal of Hydrometeorology* **14**, 829–849 (2013).

10. Dirmeyer, P. A., Sridhar Mantripragada, R. S., Gay, B. A. & Klein, D. K. D. Evolution of land surface feedbacks on extreme heat: Adapting existing coupling metrics to a changing climate. *Front. Environ. Sci.* **10**, 949250 (2022).

11. Eagleson, P. S. Climate, soil, and vegetation: 4. The expected value of annual evapotranspiration. *Water Resour. Res.* **14**, 731–739 (1978).

12. Eltahir, E. A. B. A Soil Moisture-Rainfall Feedback Mechanism: 1. Theory and observations. *Water Resour. Res.* **34**, 765–776 (1998).

13. Eltahir, E. A. B. & Bras, R. L. Precipitation recycling. *Rev. Geophys.* **34**, 367–378 (1996).

14.

638 Entekhabi, D., Rodriguez-Iturbe, I. & Castelli, F. Mutual interaction of soil
639 moisture state and atmospheric processes. *Journal of Hydrology* **184**, 3–17
640 (1996).
641 15.
642 Eyring, V. *et al.* Overview of the Coupled Model Intercomparison Project Phase 6
643 (CMIP6) experimental design and organization. *Geosci. Model Dev.* **9**, 1937–
644 1958 (2016).
645 16.
646 Feldman, A. F., Short Gianotti, D. J., Trigo, I. F., Salvucci, G. D. & Entekhabi, D.
647 Observed Landscape Responsiveness to Climate Forcing. *Water Resources*
648 *Research* **58**, (2022).
649 17.
650 Findell, K. L. & Eltahir, E. A. B. An analysis of the soil moisture-rainfall
651 feedback, based on direct observations from Illinois. *Water Resour. Res.* **33**, 725–
652 735 (1997).
653 18.
654 Fischer, E. M., Seneviratne, S. I., Lüthi, D. & Schär, C. Contribution of
655 land-atmosphere coupling to recent European summer heat waves. *Geophys. Res.*
656 *Lett.* **34**, L06707 (2007).
657 19.
658 Froidevaux, P., Schlemmer, L., Schmidli, J., Langhans, W. & Schär, C. Influence
659 of the Background Wind on the Local Soil Moisture–Precipitation Feedback.
660 *Journal of the Atmospheric Sciences* **71**, 782–799 (2014).
661 20.
662 Guillod, B. P., Orlowsky, B., Miralles, D. G., Teuling, A. J. & Seneviratne, S. I.
663 Reconciling spatial and temporal soil moisture effects on afternoon rainfall. *Nat*
664 *Commun* **6**, 6443 (2015).
665 21.
666 Hirschi, M., Mueller, B., Dorigo, W. & Seneviratne, S. I. Using remotely sensed
667 soil moisture for land–atmosphere coupling diagnostics: The role of surface vs.
668 root-zone soil moisture variability. *Remote Sensing of Environment* **154**, 246–252
669 (2014).
670 22.
671 Hirschi, M. *et al.* Observational evidence for soil-moisture impact on hot
672 extremes in southeastern Europe. *Nature Geosci* **4**, 17–21 (2011).
673 23.
674 Hsu, H. & Dirmeyer, P. A. Nonlinearity and Multivariate Dependencies in the
675 Terrestrial Leg of Land-Atmosphere Coupling. *Water Res.* **57**, (2021).
676 24.
677 Hsu, H. & Dirmeyer, P. A. Deconstructing the soil moisture-latent heat flux
678 relationship: the range of coupling regimes experienced and the presence of
679 nonlinearity within the sensitive regime. *Journal of Hydrometeorology* **1**, (2022).
680 25.
681 Hsu, H., Lo, M.-H., Guillod, B. P., Miralles, D. G. & Kumar, S. Relation between
682 precipitation location and antecedent/subsequent soil moisture spatial patterns:
683 Precipitation-Soil Moisture Coupling. *J. Geophys. Res. Atmos.* **122**, 6319–6328
684 (2017).
685 26.

686 Huszár, T., Mika, J., Lóczy, D., Molnár, K. & Kertész, Á. Climate change and
687 soil moisture: A case study. *Physics and Chemistry of the Earth, Part A: Solid*
688 *Earth and Geodesy* **24**, 905–912 (1999).
689 27.
690 Koster, R. D., Schubert, S. D. & Suarez, M. J. Analyzing the Concurrence of
691 Meteorological Droughts and Warm Periods, with Implications for the
692 Determination of Evaporative Regime. *Journal of Climate* **22**, 3331–3341 (2009).
693 28.
694 Koster, R. D., Schubert, S. D. & Suarez, M. J. Analyzing the Concurrence of
695 Meteorological Droughts and Warm Periods, with Implications for the
696 Determination of Evaporative Regime. *Journal of Climate* **22**, 3331–3341 (2009).
697 29.
698 Koster, R. D. *et al.* Regions of Strong Coupling Between Soil Moisture and
699 Precipitation. *Science* **305**, 1138–1140 (2004).
700 30.
701 Koster, R. D. & Milly, P. C. D. The Interplay between Transpiration and Runoff
702 Formulations in Land Surface Schemes Used with Atmospheric Models. *J.*
703 *Climate* **10**, 1578–1591 (1997).
704 31.
705 Koster, R. D. *et al.* GLACE: The Global Land–Atmosphere Coupling Experiment.
706 Part I: Overview. *Journal of Hydrometeorology* **7**, 590–610 (2006).
707 32.
708 Lo, M.-H. *et al.* Temporal Changes in Land Surface Coupling Strength: An
709 Example in a Semi-Arid Region of Australia. *Journal of Climate* **34**, 1503–1513
710 (2021).
711 33.
712 Lorenz, D. J. & DeWeaver, E. T. The Response of the Extratropical Hydrological
713 Cycle to Global Warming. *Journal of Climate* **20**, 3470–3484 (2007).
714 34.
715 Lorenz, R., Pitman, A. J., Hirsch, A. L. & Srbinovsky, J. Intraseasonal versus
716 Interannual Measures of Land–Atmosphere Coupling Strength in a Global
717 Climate Model: GLACE-1 versus GLACE-CMIP5 Experiments in ACCESS1.3b.
718 *Journal of Hydrometeorology* **16**, 2276–2295 (2015).
719 35.
720 Miralles, D. G., Gentine, P., Seneviratne, S. I. & Teuling, A. J. Land-atmospheric
721 feedbacks during droughts and heatwaves: state of the science and current
722 challenges: Land feedbacks during droughts and heatwaves. *Ann. N.Y. Acad. Sci.*
723 **1436**, 19–35 (2019).
724 36.
725 Miralles, D. G., Teuling, A. J., van Heerwaarden, C. C. & Vilà-Guerau de
726 Arellano, J. Mega-heatwave temperatures due to combined soil desiccation and
727 atmospheric heat accumulation. *Nature Geosci* **7**, 345–349 (2014).
728 37.
729 Santanello, J. A. *et al.* Land–Atmosphere Interactions: The LoCo Perspective.
730 *Bulletin of the American Meteorological Society* **99**, 1253–1272 (2018).
731 38.
732 Santanello, J. A., Friedl, M. A. & Ek, M. B. Convective Planetary Boundary
733 Layer Interactions with the Land Surface at Diurnal Time Scales: Diagnostics and
734 Feedbacks. *Journal of Hydrometeorology* **8**, 1082–1097 (2007).
735 39.

Santanello, J. A., Friedl, M. A. & Kustas, W. P. An Empirical Investigation of Convective Planetary Boundary Layer Evolution and Its Relationship with the Land Surface. *Journal of Applied Meteorology* **44**, 917–932 (2005).

40. Schär, C., Lüthi, D., Beyerle, U. & Heise, E. The Soil–Precipitation Feedback: A Process Study with a Regional Climate Model. *J. Climate* **12**, 722–741 (1999).

41. Schumacher, D. L., Keune, J., Dirmeyer, P. & Miralles, D. G. Drought self-propagation in drylands due to land–atmosphere feedbacks. *Nat. Geosci.* **15**, 262–268 (2022).

42. Schwingshackl, C., Hirschi, M. & Seneviratne, S. I. Quantifying Spatiotemporal Variations of Soil Moisture Control on Surface Energy Balance and Near-Surface Air Temperature. *Journal of Climate* **30**, 7105–7124 (2017).

43. Seneviratne, S. I. *et al.* Investigating soil moisture–climate interactions in a changing climate: A review. *Earth-Science Reviews* **99**, 125–161 (2010).

44. Seneviratne, S. I., Lüthi, D., Litschi, M. & Schär, C. Land–atmosphere coupling and climate change in Europe. *Nature* **443**, 205–209 (2006).

45. Short Gianotti, D. J., Rigden, A. J., Salvucci, G. D. & Entekhabi, D. Satellite and Station Observations Demonstrate Water Availability's Effect on Continental-Scale Evaporative and Photosynthetic Land Surface Dynamics. *Water Resour. Res.* **55**, 540–554 (2019).

46. Short Gianotti, D. J., Rigden, A. J., Salvucci, G. D. & Entekhabi, D. Satellite and Station Observations Demonstrate Water Availability's Effect on Continental-Scale Evaporative and Photosynthetic Land Surface Dynamics. *Water Resour. Res.* **55**, 540–554 (2019).

47. Soares, P. M. M., Careto, J. A. M., Cardoso, R. M., Goergen, K. & Trigo, R. M. Land-Atmosphere Coupling Regimes in a Future Climate in Africa: From Model Evaluation to Projections Based on CORDEX-Africa. *J. Geophys. Res. Atmos.* **124**, 11118–11142 (2019).

48. Taylor, C. M., de Jeu, R. A. M., Guichard, F., Harris, P. P. & Dorigo, W. A. Afternoon rain more likely over drier soils. *Nature* **489**, 423–426 (2012).

49. Taylor, C. M. & Ellis, R. J. Satellite detection of soil moisture impacts on convection at the mesoscale. *Geophys. Res. Lett.* **33**, L03404 (2006).

50. Ukkola, A. M., Pitman, A. J., Donat, M. G., De Kauwe, M. G. & Angélil, O. Evaluating the Contribution of Land-Atmosphere Coupling to Heat Extremes in CMIP5 Models. *Geophys. Res. Lett.* **45**, 9003–9012 (2018).

51. Vargas Zeppetello, L. R., Battisti, D. S. & Baker, M. B. The Origin of Soil Moisture Evaporation "Regimes". *Journal of Climate* **32**, 6939–6960 (2019).

52.

Yin, J., Albertson, J. D., Rigby, J. R. & Porporato, A. Land and atmospheric controls on initiation and intensity of moist convection: CAPE dynamics and LCL crossings. *Water Resour. Res.* **51**, 8476–8493 (2015).

53. Zaitchik, B. F., Macalady, A. K., Bonneau, L. R. & Smith, R. B. Europe's 2003 heat wave: a satellite view of impacts and land–atmosphere feedbacks. *Int. J. Climatol.* **26**, 743–769 (2006).

54. Zhang, J., Wang, W.-C. & Wei, J. Assessing land-atmosphere coupling using soil moisture from the Global Land Data Assimilation System and observational precipitation. *J. Geophys. Res.* **113**, D17119 (2008).

55. Zhou, S. *et al.* Soil moisture–atmosphere feedbacks mitigate declining water availability in drylands. *Nat. Clim. Chang.* **11**, 38–44 (2021).

56. Climate and Life, Volume 18 - 1st Edition. https://www.elsevier.com/books/climate-and-life/budyko/978-0-12-139450-9.

57. ***Under revision***. Hsu, H. & Dirmeyer, P. A, 2023: Soil moisture-evaporation coupling shifts into new gears under increasing CO2. Nature Communications. preprint doi:10.21203/rs.3.rs-1713539/v1